

Non-Abelian gauge fields and topological insulators in shaken optical lattices

Philipp Hauke,^{1,*} Olivier Tieleman,¹ Alessio Celi,¹ Christoph Ölschläger,² Juliette Simonet,² Julian Struck,² Malte Weinberg,² Patrick Windpassinger,² Klaus Sengstock,² Maciej Lewenstein,^{1,3} and André Eckardt⁴

¹*ICFO – Institut de Ciències Fotòniques, Parc Mediterrani de la Tecnologia, E-08860 Castelldefels, Spain*

²*Institut für Laserphysik, Universität Hamburg, Luruper Chaussee 149, D-22761 Hamburg, Germany*

³*ICREA – Institució Catalana de Recerca i Estudis Avançats, Lluís Companys 23, E-08010 Barcelona, Spain*

⁴*Max-Planck-Institut für Physik komplexer Systeme, Nöthnitzer Str. 38, D-01187 Dresden, Germany*

(Dated: July 30, 2018)

Time-periodic driving like lattice shaking offers a low-demanding method to generate artificial gauge fields in optical lattices. We identify the relevant symmetries that have to be broken by the driving function for that purpose and demonstrate the power of this method by making concrete proposals for its application to two-dimensional lattice systems: We show how to tune frustration and how to create and control band touching points like Dirac cones in the shaken kagomé lattice. We propose the realization of a topological and a quantum spin Hall insulator in a shaken spin-dependent hexagonal lattice. We describe how strong artificial magnetic fields can be achieved for example in a square lattice by employing superlattice modulation. Finally, exemplified on a shaken spin-dependent square lattice, we develop a method to create strong non-Abelian gauge fields.

Topological order and topological insulators [1] are currently in the center of interest of quantum physics, especially because of their possible applications in quantum information and spintronics [2]. For this reason, there is an ongoing search for feasible realizations of such systems in- and outside of solid-state physics. Here, ultracold ground-state atoms provide a promising playground [3] (although Rydberg-excited atoms [4], trapped ions [5], and photons in nano-structured materials [6] offer interesting alternatives). Typically, topological effects require ultra-strong gauge fields or spin-orbit-like couplings. There are several ways to achieve these with ultracold atoms, from trap rotation [7], microrotation [8], to Berry phase imprinting [9]. In optical lattices, combining laser-induced tunneling with superlattice techniques allows for strong Abelian [10] and non-Abelian [11] gauge-fields and for the realization of topological insulators [12]. So far, the first lattice experiments led to the creation of staggered flux lattices [13]. Many other groups follow this direction of research [14].

Recently, there has been a burst of interest in another, experimentally less demanding, approach, namely periodic lattice shaking. Sinusoidal shaking leads to a change of strength, or even sign of the tunneling and allows to control the Mott-insulator–superfluid transition [15, 16] (for a recent work in hexagonal geometry, see [17]). While in the square lattice this introduces neither frustration nor synthetic gauge fields, in the triangular lattice a sign-change of the tunneling is equivalent to a π -flux Abelian field [18]. Such a system mimics frustrated antiferromagnetism, classical for weakly interacting bosons [19], and quantum in the hard-core boson limit [20], where it is expected to exhibit exotic spin-liquid phases [21]. Recently, it was demonstrated that by breaking temporal symmetries of the shaking trajectory, one can cre-

ate phases of the tunneling in an optical lattice [22, 23] (see also Ref. [24]), and that in this way tunable Abelian fluxes through triangular plaquettes may be generated [22]. In this letter, we discuss non-trivial generalizations of this approach that involve also AC-induced tunneling and spinful particles. This allows us to simulate Abelian and even non-Abelian SU(2) gauge-fields in different lattice geometries, as well as topological insulators. To this, we employ non-standard optical lattices, like kagomé and spin-dependent square and hexagonal lattices, and consider scenarios based on superlattice modulation.

Basic scheme, and temporal symmetries. We consider a system of ultracold atoms in a driven optical lattice described by the Hubbard Hamiltonian $\hat{H}(t) = -\sum_{\langle ij \rangle} J_{ij} \hat{a}_i^\dagger \hat{a}_j + \sum_i v_i(t) \hat{n}_i + \hat{H}_{\text{os}}$ with (bare) tunneling matrix elements J_{ij} and annihilation and number operators \hat{a}_i and \hat{n}_i for particles (bosons or fermions) at site i ; \hat{H}_{os} collects on-site terms describing interactions or a weak static potential. The potential $v_i(t) = v_i^\omega(t) + \nu_i \hbar \omega$ consists of two parts: a rapid periodic drive $v_i^\omega(t) = v_i^\omega(t + T)$ of frequency $\omega = 2\pi/T$ and zero time average $\langle v_i^\omega(t) \rangle_T = 0$ with $\langle \cdot \rangle_T \equiv \frac{1}{T} \int_0^T \cdot dt$; and (unlike in Ref. [22]) strong static energy offsets $\nu_i \hbar \omega$ with integers ν_i . For $\hbar \omega \gg J_{ij}$ a large energy difference $\nu_{ij} \hbar \omega \neq 0$ (here and below we use the double-index shorthand $x_i - x_j \equiv x_{ij}$) practically prohibits tunneling between i and j , unless the resonant periodic driving leads to AC-induced tunneling (ACT) [25], as it has been observed in recent experiments [26]. Later on, we will augment our model by a spin degree of freedom $s = \uparrow, \downarrow$.

A gauge transformation $\hat{U} = \exp(i \sum_i \chi_i(t) \hat{n}_i)$, where $\chi_i(t) = \chi_i^\omega(t) - \nu_i \omega t + \gamma_i$ with $\hbar \chi_i^\omega(t) = -\int_0^t d\tau v_i^\omega(\tau) + \langle \int_0^t d\tau v_i^\omega(\tau) \rangle_T$ and constants γ_i , leads to the new Hamiltonian $\hat{H}'(t) = \hat{U}^\dagger \hat{H} \hat{U} - i \hbar \hat{U}^\dagger (d_t \hat{U})$, which can be approximated by its time average $\hat{H}_{\text{eff}} \equiv -\sum_{\langle ij \rangle} J_{ij}^{\text{eff}} \hat{a}_i^\dagger \hat{a}_j + \hat{H}_{\text{os}}$ if $\hbar \omega$ is large compared to both the J_{ij} and the energy scales of \hat{H}_{os} . In this treatment, the initial energy offsets

*Electronic address: philipp.hauke@icfo.es

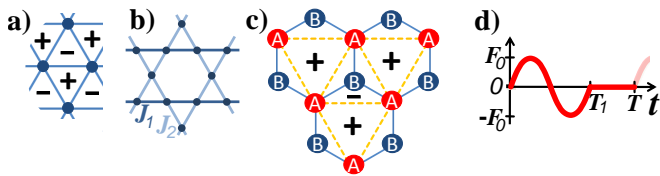


Figure 1: (color online) (a-c) Lattice geometries involving triangular plaquettes pierced by an artificial magnetic flux $\phi_{\nabla, \Delta} = \pm\phi$ (indicated by + and -): (a) triangular lattice, (b) kagomé lattice with tunneling J_1 (J_2) along the darker horizontal (lighter diagonal) bonds, and (c) hexagonal lattice with nearest-neighbor ACT (solid lines) between shallow A- and deep B-sites and next-nearest-neighbor tunneling between A-sites (dashed lines). (d) Driving function breaking symmetries (r) and (s).

$\nu_i \hbar \omega$ enter via the effective tunneling matrix elements $J_{ij}^{\text{eff}} = J_{ij} \langle e^{-i(\chi_{ij}(t))} \rangle_T$ only, and in \hat{H}_{eff} all sites appear to have the same energy. In the undriven system, for $\nu_{ij} \neq 0$, the large energy difference $\nu_{ij} \hbar \omega$ suppresses tunneling between sites i and j , and this fact is reflected in \hat{H}_{eff} by a vanishing effective tunneling $J_{ij}^{\text{eff}} = 0$ at vanishing driving $v_{ij}^{\omega} = 0$. In turn, finite driving $v_{ij}^{\omega} \neq 0$ can establish coherent ACT with $J_{ij}^{\text{eff}} \neq 0$, where the energy difference $\nu_{ij} \hbar \omega$ is bridged by ν_{ij} quanta $\hbar \omega$.

The leitmotif of the present work is to use this control scheme to induce Peierls-type phases

$$\theta_{ij} = \arg \left(\langle e^{-i(\chi_{ij}^{\omega}(t) - \nu_{ij} \omega t + \gamma_{ij})} \rangle_T \right) \quad (1)$$

that cannot be eliminated globally by choice of gauge, i.e., by adjusting the constants γ_i . Such non-trivial phases correspond to artificial Abelian gauge fields; the gauge-invariant magnetic flux $\phi_P \in (-\pi, \pi]$ piercing a lattice plaquette P is (modulo 2π) obtained by summing the θ_{ij} around P . We find that the *global* reflection symmetry (r) $v_i^{\omega}(-t - \tau) = v_i^{\omega}(t - \tau)$ with respect to a global time τ (using the choice $\gamma_i = -\nu_i \omega \tau$) implies trivial $\theta_{ij} = 0$. Moreover, if ACT is not involved ($\nu_{ij} = 0$), $\theta_{ij} = 0$ follows already from the *local* reflection symmetry (r') $v_{ij}^{\omega}(-t - \tau_{ij}) = v_{ij}^{\omega}(t - \tau_{ij})$ with independent local times τ_{ij} (since $\gamma_{ij} = \nu_{ij} \omega \tau = 0$, independent of τ), or from the shift antisymmetry (s) $v_i^{\omega}(t - \frac{T}{2}) = -v_i^{\omega}(t)$ (choosing $\gamma_i = 0$) [27]. Therefore, ACT significantly reduces the constraints on the driving function $v_i^{\omega}(t)$ for the creation of artificial magnetic fields. This is nicely exemplified by recent proposals where already simple sinusoidal forcing [fulfilling (r') and (s)] leads to magnetic fields when combined with ACT – provided the temporal phase of the driving can be made site dependent [thus breaking (r)] [29]. In the following, we consider experimentally feasible scenarios where the whole system is driven in phase [such that both (r) and (s) are broken].

We will later generalize the scheme described in the two preceding paragraphs to the case of spin-1/2 particles and show how non-Abelian gauge fields can be realized.

Homogeneous forcing and triangular plaquettes. Let us consider a homogeneous time-periodic force $\mathbf{F}(t)$, such

as an inertial force created by shaking the lattice along a periodic orbit. For $\nu_i = 0$, the driving potential $v_i^{\omega}(t) = -\mathbf{r}_i \cdot \mathbf{F}(t)$ (with site position \mathbf{r}_i) results in Peierls phases θ_{ij} that only depend on the vector $\mathbf{r}_{ij} = \mathbf{r}_i - \mathbf{r}_j$ connecting the two sites i and j , $\theta_{ij} = f(\mathbf{r}_{ij})$. Using Eq. (1), one finds that $f(-\mathbf{r}_{ij}) = -f(\mathbf{r}_{ij})$ and, therefore, homogeneous forcing cannot be used to create artificial magnetic fluxes through plaquettes with pairwise parallel edges. Since, however, generically θ_{ij} depends in a non-linear fashion on \mathbf{r}_{ij} [$f(\mathbf{r}_{ij})$ is not of the form $\mathbf{b} \cdot \mathbf{r}_{ij}$], one can use lattice shaking to induce a strong and tunable artificial magnetic flux ϕ_{∇} through, e.g., a downwards pointing triangular plaquette ∇ . In the supplemental material [30], we analytically compute this flux for unidirectional forcing. The inversion of the triangular plaquette $\nabla \rightarrow \Delta$ reverses the sign of the flux, $\phi_{\Delta} = -\phi_{\nabla}$, such that staggered fluxes can be achieved in the triangular or kagomé lattice as shown in Fig. 1a and b. Since these flux configurations stem from homogeneous forcing they do not break the translational symmetry of the lattice.

Tuning the staggered flux allows one to continuously control the degree of frustration in these lattices from none for zero-flux to maximum for π -flux [corresponding to ferromagnetic ($-J_{ij}^{\text{eff}} < 0$) and antiferromagnetic coupling ($-J_{ij}^{\text{eff}} > 0$), respectively]. The fully-frustrated regime gives rise to intriguing physics. For example, the flat lowest band of the kagomé lattice makes the system extremely susceptible towards interaction-driven physics [31]; moreover, the case of hard-core bosons can be mapped to the spin-1/2-XY antiferromagnet [20] with possible spin-liquid ground states in the spatially anisotropic triangular lattice [21] and still unexplored behavior in the kagomé geometry. The ability to tune continuously between zero and maximum frustration described here can, thus, be a powerful tool for the adiabatic preparation of frustrated quantum phases.

The realization of tunable staggered fluxes as shown in Fig. 1a and b is also interesting in its own right. In the bosonic case, deviations from π -flux directly map to tunable Dzyaloshinskii-Moriya couplings in the spin picture (see, e.g., [32]). Furthermore, for finite flux $\phi_{\Delta} = \phi$, the three bands of the kagomé lattice feature a complex band-touching structure whose topology can be controlled by the driving. This is illustrated in Fig. 2a for a lattice with $|J_{ij}^{\text{eff}}|$ equal to J_1 (J_2) along the horizontal (other) bonds (see Fig. 1b).

Topological and quantum spin Hall insulator. Such triangular plaquette fluxes can be used to engineer a topological insulator and a quantum spin Hall insulator. Consider a spin-dependent hexagonal optical lattice as sketched in Fig. 1c, where sites of the A (B) sublattice are energetically lifted (lowered) by $\Delta E/2$ for \uparrow particles, and vice versa for \downarrow particles [33]. Let us focus on non-interacting \uparrow -particles first. For substantial detuning ΔE , we can assume that nearest-neighbor (NN) tunneling (between A and B sites) is energetically suppressed and that next-NN (NNN) tunneling is relevant only between sites of the “shallow” A sublattice. Now assume

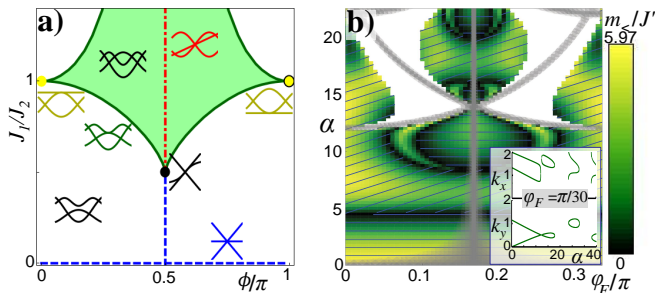


Figure 2: (color online) (a) The topology of band touching for the kagomé lattice can be controlled by anisotropy J_1/J_2 and plaquette flux ϕ . The way and how often the three bands touch is depicted by the iconographic symbols. (b) Phase diagram of the hexagonal lattice as in Fig. 1c with bare/undriven (next) nearest neighbor tunneling matrix elements J (J'), subjected to a symmetry-breaking force of amplitude α and direction $\mathbf{e}_F = \cos(\varphi_F)\mathbf{e}_x + \sin(\varphi_F)\mathbf{e}_y$, $F(t)$. white: no Dirac points are present; gray: a small nearest-neighbor tunneling $< 0.02J$ renders the physics effectively 1D. The colorbar encodes the masses at two Dirac points, labeled as $|m_{<math>| \leq |m_{>math>|}$. In the diagonally (horizontally) hatched region both masses are positive (negative). When the masses have opposite sign (un-hatched), the system is a topological insulator (or a quantum spin Hall insulator for two spin states). Inset: Position of Dirac points in k -space for $\varphi_F = \pi/30$, indicating how they move and merge with α .

that the system is driven resonantly by a time-periodic homogeneous force of frequency $\nu_{AB}\hbar\omega = \Delta E$ (with integer ν_{AB}) that both establishes NN ACT and creates finite artificial fluxes through the triangular NNN plaquettes of the A sublattice (“+” and “-” in Fig. 1c). Introducing Pauli matrices σ for the sublattice degree of freedom, the effective Hamiltonian in momentum representation becomes $\hat{H}_{\text{eff}} = \sum_{\mathbf{k}} \hat{\mathbf{a}}_{\mathbf{k}}^\dagger h(\mathbf{k}) \hat{\mathbf{a}}_{\mathbf{k}}$ where $\hat{\mathbf{a}}_{\mathbf{k}}^\dagger = (\hat{a}_{A\mathbf{k}}^\dagger, \hat{a}_{B\mathbf{k}}^\dagger)$ and $h(\mathbf{k}) = \Re(g(\mathbf{k}))\sigma_x - \Im(g(\mathbf{k}))\sigma_y + g'(\mathbf{k})\frac{1}{2}(\mathbb{1} + s_z\sigma_z)$. Here, $s_z = 1$ and $g^{(\prime)}(\mathbf{k}) \equiv -\sum_{\delta^{(\prime)}} J_{\delta^{(\prime)}}^{\text{eff}} \exp(i\mathbf{k} \cdot \boldsymbol{\delta}^{(\prime)})$ with $\boldsymbol{\delta}^{(\prime)}$ denoting the three (six) vectors connecting an A site to its NN (NNN). Diagonalizing $h(\mathbf{k})$ gives the dispersion relations $\varepsilon_{\pm}(\mathbf{k}) = \frac{1}{2}g'(\mathbf{k}) \pm \sqrt{|g(\mathbf{k})|^2 + |g'(\mathbf{k})/2|^2}$ for the two bands.

Without NNN tunneling ($g' = 0$), the system can possess a pair of band-touching points, i.e., $g(\mathbf{k}_{1,2}) = 0$, with light-cone-like dispersion relation, so-called Dirac cones. A finite NNN $g'(\mathbf{k})$ will split the bands at these points, and the Dirac-type dispersion relations found near $\mathbf{k}_{1,2}$ acquire finite “masses” $m_{1,2} = g'(\mathbf{k}_{1,2})$. If these have opposite sign, the lowest band possesses a finite Chern number (± 1). Then, if the lowest band is entirely filled with \uparrow fermions, the system is a topological insulator with quantized Hall conductivity and robust chiral edge modes [34] (see also [35]). Repeating the above reasoning for \downarrow particles, for which the role of A and B sites is interchanged, one obtains the same result, but with $s_z = -1$ and inverted Hall conductivity. Therefore, filling the lowest band with both \uparrow and \downarrow particles the system becomes a quantum spin Hall insulator with opposite chirality for

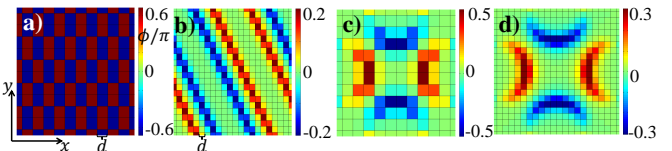


Figure 3: (color online) Artificial magnetic fluxes ϕ through the plaquettes of a square lattice (lattice constant d , indicated by the grid) resulting from superlattice modulation. Stripes or larger patches with strong, rectified magnetic fluxes can be achieved. (a) and (b): Single-component superlattices with (a) $\mathbf{q}_1 = (\pi/d)(\mathbf{e}_x + \mathbf{e}_y/2)$, $V_1 = 4\hbar\omega$; (b) $\mathbf{q}_1 = \frac{1}{10}(\pi/d)(\mathbf{e}_x + \mathbf{e}_y/2)$ and $V_1 = 20\hbar\omega$. (c): Two components with $\mathbf{q}_{1/2} = \frac{1}{10}(\pi/d)(\mathbf{e}_x \pm \mathbf{e}_y)$, $V_{1/2} = 12\hbar\omega$. (d): Like (c), but with wavelengths and amplitudes doubled. Always $\varphi_s = 0$.

the two species [36].

As an example, we consider unidirectional forcing $\mathbf{F}(t) = F(t)\mathbf{e}_F$, with $\mathbf{e}_F = \cos(\varphi_F)\mathbf{e}_x + \sin(\varphi_F)\mathbf{e}_y$ and $F(t)$ as depicted in Fig. 1d (with $T_1 = T/2$ and $\hbar\omega = \Delta E/2$, see supplemental material [30] for an analytical expression of the resulting phases). By varying the angle φ_F and the forcing strength $\alpha = dF_0T_1/(2\pi\hbar)$ (with lattice constant d), we can access various topological quantum phase transitions, where at least one of the masses vanishes and changes sign (Fig. 2b). Thus, the lowest band can acquire a non-trivial Chern number. The inset shows how Dirac points can be moved and merged.

A way to measure the topological band structure of the system is given by the method of Ref. [37] based on semi-classical wave-packet dynamics. It can be applied thanks to the adiabatic principle for Floquet systems [38] (see [39] for its application to the effective Hamiltonian).

Superlattice modulation and flux rectification. In lattices with pairwise parallel bonds, such as square lattices, homogeneous driving $v_i^\omega(t) = -\mathbf{F}(t) \cdot \mathbf{r}_i$ as considered in the previous paragraphs cannot create magnetic fluxes. Therefore, we propose to drive the system via an oscillating superlattice potential $v_i(t) = f(t)V_0(\mathbf{r}_i) = f(t)\sum_s \frac{V_s}{2} \cos(\mathbf{q}_s \cdot \mathbf{r} - \varphi_s)$, where $V_0(\mathbf{r})$ may be incommensurate with the host lattice. The driving function $f(t) = f(t+T)$ breaks symmetries (r) and (s). To achieve a vanishing mean, $\langle f(t) \rangle_T = 0$, in an experiment one can use π -shifted non-interfering standing waves such that $f(t)V_s \cos(\mathbf{q}_s \cdot \mathbf{r} - \varphi_s) = V'_s(t) \cos(\mathbf{q}_s \cdot \mathbf{r} - \varphi_s) + V''_s(t) \cos(\mathbf{q}_s \cdot \mathbf{r} - \varphi_s + \pi)$, with $V'_s, V''_s > 0$. In Fig. 3, we show – on the example of a square lattice with a shaking function as in Fig. 1d (with $T_1/T = 0.8$) – that, using different superlattice structures, various configurations of plaquette fluxes can be engineered [40]. Roughly, the larger the superlattice wavelengths the slower is the variation of the artificial flux. Therefore, superlattice modulation can generate not only strong magnetic fluxes through square plaquettes, but also large regions (stripes or patches) with rectified magnetic field where strong-field quantum Hall-type physics can be studied. Their inhomogeneity and finite extent provide a promising test ground for the investigation of robust edge modes.

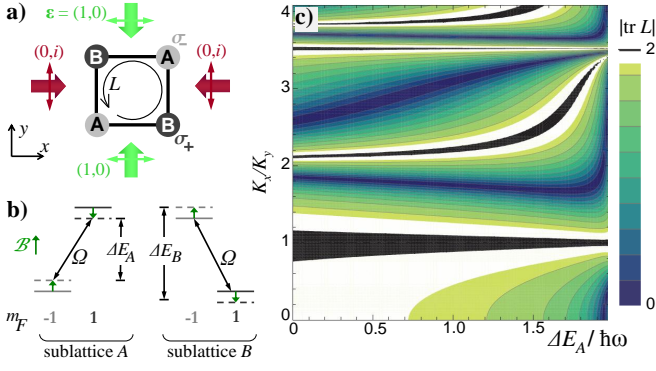


Figure 4: (color online) Non-Abelian SU(2) gauge fields. (a) Two standing laser waves (with a phase shift of $\pi/2$ and in-plane polarization as denoted in the figure) create a bipartite square lattice with alternating σ^+ and σ^- polarized sites (A and B) [41]. $m_F = \pm 1$ particles feel an energy difference of $\pm\Delta E$ between A and B sites. (b) The resulting level scheme. A constant B-field realizes an additional on-site energy splitting $\Delta E'$ (green arrow) such that $|\Delta E_{A,B}| = |\pm\Delta E + \Delta E'|$ becomes sublattice dependent. The coupling Ω of both spin states can be realized by magnetic or microwave fields. (c) Trace of the Wilson loop L in parameter space. Deviations from 2 imply non-Abelian physics [$K_y = 1.814$; outside the white (black) regions, $|\text{tr}L| < 1.9$ (< 1.99)].

Non-Abelian SU(2) gauge fields. The periodic driving also permits the creation of arbitrary *non-Abelian* SU(2) gauge fields. Consider \uparrow and \downarrow particles (say, $m_F = \pm 1$) loaded into the spin-dependent square lattice depicted in Fig. 4a, where the energy of \uparrow particles is lifted (lowered) by $\Delta E/2$ on A (B) sites, and vice versa for \downarrow particles. These energy shifts are summarized by $\Delta E\sigma_z s_z/2$, if we introduce two sets of Pauli matrices s and σ for spin (\uparrow or \downarrow) and sublattice (A or B), respectively. Moreover, uniform microwave and magnetic fields can be employed to couple the \uparrow and \downarrow state with a matrix element Ω and to produce an additional site-independent energy splitting $\Delta E'$, giving the site-independent term $\Delta E' s_z/2 + \Omega s_x$. The absolute value of the total \uparrow - \downarrow splitting $\Delta E_i = \Delta E\sigma_z - \Delta E'$ is sublattice-dependent (Fig. 4b). Including the NN tunneling J and a spin-independent sinusoidal drive $v_i^\omega(t) = -\mathbf{r}_i \cdot \mathbf{F}_0 \cos(\omega t)$ as it can be induced by simply shaking the lattice back and forth, the Hamiltonian reads $\hat{H} = -\sum_{\langle ij \rangle} J \hat{\mathbf{a}}_i^\dagger \hat{\mathbf{a}}_j + \sum_i \hat{\mathbf{a}}_i^\dagger [\frac{1}{2} \Delta E_i s_z + \Omega s_x + v_i^\omega(t)] \hat{\mathbf{a}}_i$, with $\hat{\mathbf{a}}_i^\dagger = (\hat{a}_{i\uparrow}^\dagger, \hat{a}_{i\downarrow}^\dagger)$. The transformation $\hat{\mathbf{b}}_i = u_i^\dagger \hat{\mathbf{a}}_i$, where u_i are time-independent unitary 2×2 -matrices, diagonalizes the Hamiltonian on site with eigenvalues $\hbar\lambda_i = \frac{1}{2} \sqrt{\Delta E_i^2 + 4\Omega^2}$. This yields $\hat{H} = -\sum_{\langle ij \rangle} J \hat{\mathbf{b}}_i^\dagger u_i^\dagger u_j \hat{\mathbf{b}}_j + \sum_i \hat{\mathbf{b}}_i^\dagger [\hbar\lambda_i s_z + v_i^\omega(t)] \hat{\mathbf{b}}_i$. The sublattice dependence of u_i through $\Delta E_i/(2\Omega)$ achieves generically $u_i^\dagger u_j \neq 1$. As in the derivation preceding Eq. (1), the unitary transformation $\exp(-i \sum_i \hat{\mathbf{b}}_i^\dagger [\lambda_i t s_z - K_i \sin(\omega t)] \hat{\mathbf{b}}_i)$ with $K_i = \mathbf{r}_i \cdot \mathbf{F}_0/(\hbar\omega)$ leads to a purely kinetic Hamiltonian $\hat{H}' = -\sum_{\langle ij \rangle} J \hat{\mathbf{b}}_i^\dagger W_{ij}(t) \hat{\mathbf{b}}_j$. Here,

$$W_{ij}(t) = e^{-iK_{ij} \sin(\omega t)} \begin{pmatrix} c_{ij} e^{i(\lambda_i - \lambda_j)t} & d_{ij} e^{-i(\lambda_i + \lambda_j)t} \\ -d_{ij}^* e^{i(\lambda_i + \lambda_j)t} & c_{ij}^* e^{-i(\lambda_i - \lambda_j)t} \end{pmatrix},$$

and c_{ij} and d_{ij} parametrize $u_i^\dagger u_j$. For $\hbar\omega \gg J_{ij}$, we can approximate \hat{H}' by its time average $\hat{H}_{\text{eff}} = \langle \hat{H}' \rangle_T = -\sum_{\langle ij \rangle} J_{ij}^{\text{eff}} \hat{\mathbf{b}}_i^\dagger M_{ij} \hat{\mathbf{b}}_j$, with the effective tunneling matrix elements $J_{ij}^{\text{eff}} = J \sqrt{|\det(\langle W_{ij} \rangle_T)|}$, and the matrices $M_{ij} \equiv \langle W_{ij} \rangle_T / \sqrt{|\det(\langle W_{ij} \rangle_T)|}$. For $J_{ij}^{\text{eff}} \neq 0$, we require $\lambda_{i \in B} \pm \lambda_{i \in A} = \nu_\pm \omega$ with integers ν_\pm , and for unitarity of M_{ij} , we require ν_\pm both either odd or even.

If the so called Wilson loop L , the product of the matrices M_{ij} around a plaquette, yields not just a simple phase $e^{i\phi}$ describing an Abelian magnetic flux ϕ , the system is subjected to a genuine non-Abelian SU(2) gauge field. This is equivalent to requiring $|\text{tr}L| < 2$, a *sine qua non* for the anomalous integer quantum Hall effect [42] and fractional quantum Hall states with non-Abelian anyonic excitations [43]. Without driving, $|\text{tr}L| = 2$, but including it, $|\text{tr}L| < 2$ can be fulfilled (see [30]).

Let us choose $\nu_+ = 3$ and $\nu_- = 1$, achieved by $\Delta E_B = \sqrt{4(\hbar\omega)^2 + \Delta E_A^2}$ and $\Omega = \sqrt{(\hbar\omega)^2 - \Delta E_A/4}$. This leaves $\Delta E_A/\hbar\omega$, K_x , and K_y as free parameters (where $K_{x,y}$ is the amplitude of the forcing K_{ij} in positive x, y -direction). In Fig. 4c, we plot the trace of the Wilson loop $|\text{tr}L|$ versus K_x/K_y and $E_A/\hbar\omega$ for $K_y = 1.84$ (this value is not crucial but ensures large y -tunneling – see supplemental material [30], where also an analytical expression for the Wilson loop is derived). There are broad regions where $|\text{tr}L|$ differs strongly from 2, proving the presence of a strong artificial non-Abelian gauge field. Under typical conditions, the system shows Dirac cones, be it Abelian or non-Abelian. Similar analytic calculations reveal that $L \equiv \mathbb{1}$ in a hexagonal lattice (and for even ν_\pm in the square lattice). This limitation can be overcome by employing position-dependent coupling via Raman laser mixing, $\Omega \rightarrow \Omega_i = \Omega e^{i\mathbf{q} \cdot \mathbf{r}_i}$ with \mathbf{q} the laser wave-vector difference (see [30]). This way, the M_{ij} as well as L can be tuned to be a generic ($i \times$) SU(2) matrix both in square and hexagonal lattices. Alternatively, in a hexagonal lattice a non-trivial Wilson loop can be achieved with NNN tunneling.

Conclusion. The creation of artificial Abelian and non-Abelian gauge fields by means of time-periodic forcing opens realistic perspectives for experimental studies. This method offers great flexibility, because it does not involve the internal atomic structure. For fermions, where only different internal states interact with each other, this can be very advantageous for reaching the strongly correlated regime.

Acknowledgments We acknowledge support from AAIL-Hubbard, Spanish MICINN (FIS2008-00784), Catalunya-Caixa, EU Projects AQUITE and NAME-QUAM, ERC grant QUAGATUA, Netherlands Organisation for Scientific Research (NWO), Humboldt Stiftung, German Science foundation (grants FOR 801 and SFB 925), and Hamburg Theory Prize.

- [1] M. Z. Hasan and C. L. Kane, *Rev. Mod. Phys.* **82**, 3045 (2010).
- [2] C. Nayak, *et al.*, *Rev. Mod. Phys.* **80**, 1083 (2008).
- [3] M. Lewenstein, A. Sanpera, and V. Ahufinger, *Ultracold Atoms in Optical Lattices: Simulating Quantum Many-Body Systems*. Oxford University Press, Oxford, (2012).
- [4] H. Weimer, *et al.*, *Nat. Phys.* **6**, 382 (2010).
- [5] J. T. Barreiro, *et al.*, *Nature* **470**, 486 (2011).
- [6] T. Kitagawa, *et al.*, *Nat. Commun.* **3**, 882 (2012). A. Aspuru-Guzik and P. Walther, *Nat. Phys.* **8**, 285 (2012).
- [7] A. L. Fetter, *Rev. Mod. Phys.* **81**, 647 (2009).
- [8] A. S. Sørensen, E. Demler, and M. D. Lukin, *Phys. Rev. Lett.* **94** 086803 (2005); L.-K. Lim, C. Morais Smith, and A. Hemmerich, *Phys. Rev. Lett.* **100** 130402 (2008); L.-K. Lim, A. Lazarides, A. Hemmerich, and C. Morais Smith, *Phys. Rev. A* **82** 013616 (2010); T. Kitagawa, E. Berg, M. Rudner, and E. Demler, *Phys. Rev. B* **82** 235114 (2010).
- [9] J. Dalibard, F. Gerbier, G. Juzeliunas, and P. Öhberg, *Rev. Mod. Phys.* **83**, 1523 (2011); Y.-J. Lin, *et al.*, *Nature* **462**, 628 (2009); Y.-J. Lin, K. Jiménez-García, and I. B. Spielman, *Nature* **471**, 83 (2011).
- [10] D. Jaksch and P. Zoller, *New J. Phys.* **5**, 56 (2003).
- [11] K. Osterloh, *et al.*, *Phys. Rev. Lett.* **95**, 010403 (2005).
- [12] L. Mazza, *et al.*, *New J. Phys.* **14**, 015007 (2012).
- [13] M. Aidelsburger, *et al.*, *Phys. Rev. Lett.* **107**, 255301 (2011).
- [14] L. Tarruell, *et al.*, *Nature* **483**, 302 (2012); G.-B. Jo, *et al.*, *Phys. Rev. Lett.* **108**, 045305 (2012).
- [15] A. Eckardt, C. Weiss, and M. Holthaus, *Phys. Rev. Lett.* **95**, 260404 (2005).
- [16] H. Lignier, *et al.*, *Phys. Rev. Lett.* **99**, 220403 (2007); A. Zenesini, *et al.*, *Phys. Rev. Lett.* **102**, 100403 (2009).
- [17] S. Koghee, L.-K. Lim, M. O. Goerbig, and C. Morais Smith, *Phys. Rev. A* **85** 023637 (2012).
- [18] V. Kalmeyer and R. B. Laughlin, *Phys. Rev. Lett.* **59**, 2095 (1987).
- [19] J. Struck, *et al.*, *Science* **333** 996 (2011).
- [20] A. Eckardt, *et al.*, *Europhys. Lett.* **89**, 10010 (2010).
- [21] R. Schmied, *et al.*, *New J. Phys.* **10**, 045017 (2008); P. Hauke, *et al.*, *New J. Phys.* **12**, 053036 (2010).
- [22] J. Struck, *et al.*, *Phys. Rev. Lett.* **108**, 225304 (2012).
- [23] K. Sacha, K. Targońska, and J. Zakrzewski, *Phys. Rev. A* **85**, 053613 (2012).
- [24] K. Jiménez-García, *et al.*, *Phys. Rev. Lett.* **108**, 225303 (2012).
- [25] A. Eckardt and M. Holthaus, *Europhys. Lett.* **80**, 50004 (2007).
- [26] C. Sias, *et al.*, *Phys. Rev. Lett.* **100**, 040404 (2008); A. Alberti, V. V. Ivanov, G. M. Tino, and G. Ferrari, *Nat. Phys.* **5**, 547 (2009); E. Haller, *et al.*, *Phys. Rev. Lett.* **104**, 200403 (2010); R. Ma *et al.*, *Phys. Rev. Lett.* **107**, 095301 (2011).
- [27] See Refs. [22, 28] for connections to ratchet physics.
- [28] S. Flach, O. Yevtushenko, and Y. Zolotaryuk, *Phys. Rev. Lett.* **84**, 2358 (2000); S. Denisov, L. Morales-Molina, S. Flach, and P. Hänggi, *Phys. Rev. A* **75**, 063424 (2007).
- [29] A. R. Kolovsky, *Europhys. Lett.* **93**, 20003 (2011); A. Bermudez, T. Schaetz, and D. Porras, arXiv:1201.3287 (2012).
- [30] See supplemental material for an analytic calculation of J_{ij}^{eff} and θ_{ij} , and for technical details on the creation of non-Abelian SU(2) gauge fields.
- [31] S. D. Huber and E. Altman, *Phys. Rev. B* **82**, 184502 (2010).
- [32] L. Messio, O. Cepas, and C. Lhuillier, *Phys. Rev. B* **81**, 064428 (2010).
- [33] P. Soltan-Panahi, *et al.*, *Nat. Phys.* **7**, 434 (2011).
- [34] F. D. M. Haldane, *Phys. Rev. Lett.* **61**, 2015 (1988).
- [35] E. Alba, *et al.*, *Phys. Rev. Lett.* **107**, 235301 (2011); T. Kitagawa *et al.*, *Phys. Rev. B* **84**, 235108 (2011); N. Goldman *et al.*, *Phys. Rev. Lett.* **105**, 255302 (2010).
- [36] C. L. Kane and E. J. Mele, *Phys. Rev. Lett.* **95**, 226801 (2005).
- [37] H. M. Price and N. R. Cooper, *Phys. Rev. A* **85**, 033620 (2012).
- [38] H. P. Breuer and M. Holthaus, *Phys. Lett. A* **140**, 507 (1989).
- [39] A. Eckardt and M. Holthaus, *Phys. Rev. Lett.* **101**, 245302 (2008).
- [40] For long superlattice wave lengths $|\mathbf{q}_s d| \ll \pi$ (applies to Fig. 3b,c,d), the flux through a plaquette at \mathbf{r} is given by $\phi(\mathbf{r}) \simeq \frac{1}{2} w_{xy}(\mathbf{r}) [\theta'(w_y(\mathbf{r})) - \theta'(w_x(\mathbf{r}))]$, where a prime indicates the derivative, and where $w_{\mu\nu}(\mathbf{r}) = d^2 \partial_\mu \partial_\nu V(\mathbf{r}) / (\hbar\omega)$ and $w_\mu = d \partial_\mu V(\mathbf{r}) / (\hbar\omega)$.
- [41] A. Hemmerich and T. W. Hänsch, *Phys. Rev. Lett.* **70**, 410 (1993).
- [42] N. Goldman, *et al.*, *Phys. Rev. Lett.* **103**, 035301 (2009).
- [43] M. Burrello and A. Trombettoni, *Phys. Rev. Lett.* **105**, 125304 (2010).

Supplemental Material

I. ANALYTIC FORM OF THE EFFECTIVE TUNNELING AND THE PEIERLS PHASES

In the examples of the main text, we use a driving potential $\mathbf{F}(t) = F(t)\mathbf{e}_F$ which is unidirectional, i.e., $\mathbf{e}_F = \cos(\varphi_F)\mathbf{e}_x + \sin(\varphi_F)\mathbf{e}_y$, and has a paused-sine-wave amplitude as depicted in Fig. 1d,

$$F(t) = \begin{cases} F_0 \sin(2\pi t/T_1), & 0 \leq t \bmod T < T_1 \\ 0, & T_1 \leq t \bmod T < T \end{cases} \quad (\text{S1})$$

Carrying out the time integrations as given in the introduction of the main text, this driving creates – for a vanishing energy difference between sites i and j , characterized by $\nu_{ij} = 0$ – the effective tunneling

$$\frac{J_{ij}^{\text{eff}}}{J_{ij}} = \frac{T_1}{T} e^{-i\gamma_{ij}} \left[-e^{-i\alpha_{ij} \frac{T-T_1}{T}} \mathcal{J}_0(\alpha_{ij}) + e^{i\alpha_{ij} \frac{T_1}{T}} \frac{T-T_1}{T_1} \right]. \quad (\text{S2})$$

and for $\nu_{ij} \neq 0$ the AC-induced tunneling (ACT)

$$\frac{J_{ij}^{\text{eff}}}{J_{ij}} = \frac{T_1}{T} e^{-i\gamma_{ij}} \left[-e^{-i\nu_{ij} \frac{\pi}{2}} e^{-i\alpha_{ij} \frac{T-T_1}{T}} \mathcal{J}_{\nu_{ij}}(\alpha_{ij}) - \frac{i}{2\pi\nu_{ij}} e^{i\alpha_{ij} \frac{T_1}{T}} \left(e^{i2\pi\nu_{ij} \frac{T}{T_1}} - 1 \right) \right], \quad (\text{S3})$$

Here, \mathcal{J}_μ is the BesselJ function of order μ , γ_{ij} correspond to the freedom to choose the local phases, and we defined the dimensionless driving amplitude $\alpha_{ij} = \mathbf{r}_{ij} \cdot \mathbf{e}_F F_0 T_1 / (2\pi\hbar)$. For the case $T_1 = T/2$ (and choosing the local phases $\gamma_{ij} = 0$), as considered in the section *Topological and quantum spin Hall insulator*, the Peierls phases θ_{ij} are thus for nearest neighbors (NN) (where $\nu_{ij} = 1$)

$$\theta_{ij} \equiv f(\mathbf{r}_{ij}) = \frac{1}{2} (\pi - \alpha_{ij}), \quad (\text{S4})$$

and for next-NN (NNN) (where $\nu_{ij} = 0$)

$$\tan \theta_{ij} \equiv \tan f(\mathbf{r}_{ij}) = \frac{1 + \mathcal{J}_0(\alpha_{ij})}{1 - \mathcal{J}_0(\alpha_{ij})} \tan \frac{\alpha_{ij}}{2}. \quad (\text{S5})$$

The flux threaded through a triangular plaquette as sketched in Fig. 1a-b is then $\phi = f(\mathbf{e}_x) + f(-\mathbf{e}_x/2 + \sqrt{3}/2\mathbf{e}_y) + f(-\mathbf{e}_x/2 - \sqrt{3}/2\mathbf{e}_y)$ (and similarly for Fig. 1c, where the plaquette is spanned by NNN tunneling). It can be non-zero since $f(\mathbf{r}_{ij})$ is a non-linear function of \mathbf{r}_{ij} .

II. NON-ABELIAN SU(2) GAUGE FIELDS

A. Independence of the observables on the choice of the phases of the local basis

In the main text, it is shown how a non-Abelian gauge field can be induced via lattice shaking in a bipartite, spin-dependent lattice. Here, we comment on some technical and background aspects that have been omitted there. We adopt the same notation as in the main text. First, we focus on the the example of site-independent magnetic mixing $\Omega_i = \Omega, \forall i$. The on-site Hamiltonian is

$$H_i = E_i s_z + \Omega s_x, \quad (\text{S6})$$

where $E_i = E_A$, if the site i belongs to sublattice A , while $E_i = E_B$, if it belongs to sublattice B . The transformation u_i diagonalizing H_i can be written as

$$u_i = e^{\frac{i}{2}\Lambda_i s_y} e^{i(\varphi_i s_z + \tau_i)}, \quad (\text{S7})$$

where $\Lambda_i \equiv \text{atan} \frac{E_i}{\Omega}$. The phases φ_i and τ_i correspond to the γ_i ; they attest the freedom in choosing the phases of the two states which form the local basis. As these are arbitrary, physical observables – for instance the Wilson Loop operator L – cannot depend on such phases. This is immediate in the absence of periodic driving. Indeed, in that case the Wilson loop is the identity whatever choice of u_i is performed, as it corresponds to products of terms $u_i u_i^\dagger = \mathbb{1}$, for any site i in the loop. In presence of periodic driving, the cancellation of the phases is slightly more involved. Following the definition of the effective hopping matrices M_{ij} in the main text, $M_{ij} \equiv \langle W_{ij} \rangle_T / \sqrt{|\det(\langle W_{ij} \rangle_T)|}$, we notice that that their matrix elements have the same phases (up to multiples of π) as the elements $u_i^\dagger u_j = \begin{pmatrix} c_{ij} & d_{ij} \\ -d_{ij}^* & c_{ij}^* \end{pmatrix}$, while their moduli are independent of such phases. This implies that for two different choices of the local phases at the site k , φ'_k, τ'_k , and φ_k, τ_k , respectively, the effective hopping matrices relate as

$$M'_{ij} = e^{i(\Delta\varphi_i s_z + \Delta\tau_i)} M_{ij} e^{-i(\Delta\varphi_j s_z + \Delta\tau_j)}, \quad (\text{S8})$$

where $\Delta\varphi_k \equiv \varphi'_k - \varphi_k$, and $\Delta\tau_k \equiv \tau'_k - \tau_k$. That is, the choice of the phases commutes with the time-average procedure. It follows that they cancel out when the hopping matrices M_{ij} are multiplied in the Wilson Loop L as in the time-independent case. Hence, L is independent of the choice of local phases, as it should be.

We conclude by remarking that the same happens for more involved choices of the optical lattice, as the actual form of the local Hamiltonian does not play any role (cf. section II C).

B. Analytic calculation of the Wilson Loop

Here, we show how to derive analytically the Wilson Loop L computed along the fundamental plaquette for a forced lattice described by (S6). Using the result explained in the previous section, we may choose $\varphi_i = \tau_i = 0, \forall i$. Using this in (S7), this implies that

$$u_i^\dagger u_j = e^{\frac{i}{2}(\Lambda_j - \Lambda_i)s_y}. \quad (\text{S9})$$

We may call S the forcing-induced non-linear map that relates $u_i^\dagger u_j$ to the effective hopping matrix M_{ij} , $M_{ij} = S[u_i^\dagger u_j]$. Because we employed the unitary transformation $\exp(-i \sum_i \hat{\mathbf{b}}_i^\dagger [\lambda_i t s_z - K_i \sin(\omega t)] \hat{\mathbf{b}}_i)$ to arrive at Eq. (2) of the main text, this map is a function of the energy differences between A and B sites, $\lambda_{i \in B} \pm \lambda_{i \in A} = \nu_\pm \omega$. To ensure finite ACT, the ν_\pm have to be integers. Explicitly, as defined in the main text, $M_{ij} \equiv \langle W_{ij} \rangle_T / \sqrt{|\det(\langle W_{ij} \rangle_T)|}$, which yields, following Eq. (2),

$$\langle W_{ij} \rangle_T = \begin{pmatrix} c_{ij} \mathcal{J}_{\nu_-}(K_{ij}) & d_{ij} \mathcal{J}_{\nu_+}(K_{ij}) \\ d_{ij}^* \mathcal{J}_{\nu_+}(K_{ij}) & -c_{ij}^* \mathcal{J}_{\nu_-}(K_{ij}) \end{pmatrix}. \quad (\text{S10})$$

Here, the amplitude of the forcing $K_{ij} = (\mathbf{r}_i - \mathbf{r}_j) \cdot \mathbf{F}_0 / (\hbar \omega)$ depends only on the direction δ_l of link ij ($\delta_{l=1,2} = \hat{x}, \hat{y}$ for the square lattice, and $\delta_{l=1,2,3} = \hat{x}, -\frac{1}{2}(\hat{x} - \sqrt{3}\hat{y}), -\frac{1}{2}(\hat{x} + \sqrt{3}\hat{y})$ for the hexagonal one). To ensure unitarity $M_{ij} M_{ji} = \mathbb{1}$, we therefore have to impose the additional condition that the ν_\pm are either both even or both odd (use $\nu_-(ji) = -\nu_-(ij)$ and $K_{ji} = -K_{ij}$).

First, we characterize the action of S on Eq. (S9) for *even* forcing, i.e., when both ν_+ and ν_- are even numbers, $\nu_+ = 2n$, $\nu_- = 2n'$. By the observation that S maps by construction *i*) unitary matrices to unitary matrices, and *ii*) real matrices to real matrices, it follows that $S[e^{i\varphi s_y}] = e^{i\varphi' s_y}$, where $\varphi' = \text{atan}[\frac{\mathcal{J}_{2n'}(K_{ij})}{\mathcal{J}_{2n}(K_{ij})} \tan \varphi]$. The main consequence of this form of $S[e^{i\varphi s_y}]$ is that hopping matrices $M_{ij} = M_l$ commute also for different links l , and this implies that the Wilson loop for the square, $L = M_1 M_2 M_1^\dagger M_2^\dagger$, and for the hexagonal lattice $L = M_1 M_3^\dagger M_2 M_1^\dagger M_3 M_2^\dagger$, are both equal to the identity (by convention, we travel the loop on fundamental cells anticlockwise, starting from the bottom-left corner).

The situation is more interesting for *odd* forcing, i.e., when both ν_+ and ν_- are odd numbers, $\nu_+ = 2n + 1$, $\nu_- = 2n' + 1$. The result of the time-averaging is in this case $S[e^{i\varphi s_y}] = s_z e^{i\varphi' s_y}$, where $\varphi' = \text{atan}[\frac{\mathcal{J}_{2n'+1}(K_{ij})}{\mathcal{J}_{2n+1}(K_{ij})} \tan \varphi]$. Due to the presence of the s_z , for the square lattice, starting by convention from sublattice A, we get

$$\begin{aligned} L &= M_1 M_2 M_1^\dagger M_2^\dagger = \\ &= s_z e^{i\varphi'_x s_y} s_z e^{i\varphi'_y s_y} e^{-i\varphi'_x s_y} s_z e^{-i\varphi'_y s_y} s_z = e^{i(\varphi'_y - \varphi'_x) s_y}, \end{aligned}$$

where $\varphi'_\mu = \text{atan}[\frac{\mathcal{J}_{2n'+1}(K_\mu)}{\mathcal{J}_{2n+1}(K_\mu)} \tan[\frac{1}{2}(\text{atan}\frac{E^B}{\Omega} - \text{atan}\frac{E^A}{\Omega})]]$, $\mu = x, y$. As shown numerically in the main text, the

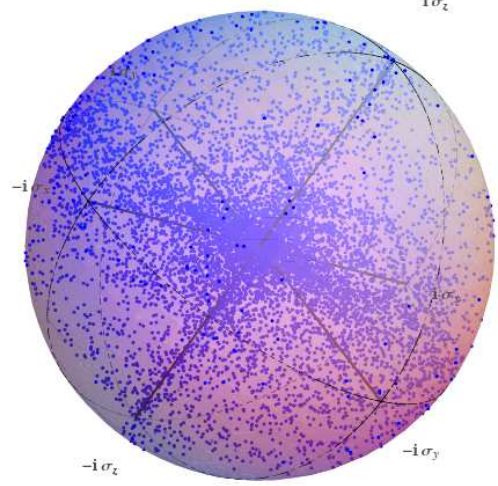


Figure S1: Bloch sphere representation of the Wilson loop L computed for odd forcing in a hexagonal lattice with $|\mathbf{q}| = 1$ (in lattice step units). E_B is taken to be $E_B = -\sqrt{4E_A^2 + 3\Omega}$ such that the eigenvalues enjoy the relation $\lambda_B = 2\lambda_A = \sqrt{E_A^2 + \Omega} = 2\omega$, which implies $\lambda_B + \lambda_A = 3\omega$, and $\lambda_B - \lambda_A = \omega$. Here, ω is the frequency of the periodic forcing. The parameters $\mathbf{q} = (\cos \theta_q, \sin \theta_q)$, the intensity of the shaking $\mathbf{K} = |\mathbf{K}|(\cos \theta_K, \sin \theta_K)$, and E_A , are chosen randomly in the ranges, $\theta_q \in [0, 2\pi[$, $|\mathbf{K}| \in]0, 5[$, $\theta_K \in [0, 2\pi[$, and $\frac{E_A}{\Omega} \in]5, 15[$, respectively. The resulting L 's cover the entire Bloch sphere.

difference $\varphi'_y - \varphi'_x$ can take any value between zero and 2π , allowing for a non-trivial Wilson Loop, $\text{tr}|L| = 2|\cos(\varphi'_y - \varphi'_x)| \neq 2$. In the example, we have chosen $K_y = 1.84$, because this lies close to the first maximum of the BesselJ function $\mathcal{J}_1(K_y)$, ensuring large tunneling $J_{ij}^{\text{eff}} = J\sqrt{|\det(\langle W_{ij} \rangle_T)|}$ in y -direction.

On the other hand, for the hexagonal lattice we get always a trivial result as the s_z 's cancel out and $L = \mathbb{1}$.

C. Raman-induced mixing

Considering a site-independent mixing of \uparrow - and \downarrow -particles as in (S6), the form of M_{ij} is limited to $e^{i\varphi' s_y}$ or $s_z e^{i\varphi' s_y}$. This can be circumvented by considering site-dependent Raman mixing. In this case, the local Hamiltonian takes the form

$$H_i = E_i s_z + \Omega [\cos(\mathbf{q} \cdot \mathbf{r}_i) s_x - \sin(\mathbf{q} \cdot \mathbf{r}_i) s_y], \quad (\text{S11})$$

where \mathbf{q} is the difference of the wave vector of the two Raman lasers, $E_i = E_A, \forall i \in A$, and $E_i = E_B, \forall i \in B$.

The main difference in this case is that, while still depending only on the link direction $\mathbf{r}_i - \mathbf{r}_j$, the M_{ij} for different link directions are generally not commuting. Indeed, in this case the local transformation u_i may be cho-

sen as $u_i = e^{i\frac{\mathbf{q}\cdot\mathbf{r}_i}{2}s_z} e^{i\frac{1}{2}\text{atan}\frac{E_i}{\Omega}s_y}$. Hence, considering a site j and all its neighbors i , the products $u_i^\dagger u_j$ for different link directions are not commuting, and the map S acts highly non-trivial on them. Numerical studies with

random selected parameters (Fig. S1) show that the corresponding Wilson Loop L is in general non-trivial and dense in the Bloch sphere, i.e., we can simulate any designed $L \in \text{SU}(2)$, not just matrices of the form $e^{i\theta s_y}$.